CCUS: 4016392

Aqueous Nanobubble Dispersion of CO_2 in Sodium Formate Solution for Enhanced CO_2 Mineralization Using Basaltic Rocks

Hao Wang*[1], Omar A. Carrasco-Jaim[1], Ryosuke Okuno[1], 1. The University of Texas at Austin, Austin, Texas 78712, USA.

Abstract

This paper presents an experimental study of carbon dioxide (CO_2) mineralization by injecting aqueous nanobubble dispersion of CO_2 into crushed basaltic rock samples at 75°C. Two CO_2 nanobubble fluids were compared: one with deionized (DI) water and the other with 30 wt% sodium formate solution (20 wt% formate). Each injection was initialized by saturating the rock sample container with DI water without CO_2 content. The main objectives of this research were to test two mechanisms of mineral dissolution, proton-promoted and ligand-promoted mechanisms, and their effects on the subsequent CO_2 mineralization with metal silicates in basaltic rock samples.

The experimental program in this research included measurements of CO_2 contents in aqueous nanobubble dispersions, static experiments of mineral dissolution by sodium formate solutions at different concentrations, and dynamic flow-through experiments of mineral dissolution and CO_2 mineralization by the two injection fluids mentioned previously.

Aqueous nanobubble dispersion enabled the water phase to be saturated with CO_2 at a higher level than the inherent solubility of CO_2 at 75°C. At 138.9 bara, the CO_2 concentration in the nanobubble fluid with DI water was 1.75 mol/L, which was 65% greater than the inherent solubility at the same temperature and pressure. The dynamic flow-through experiments with CO_2 nanobubble dispersion in DI water (Case #1) resulted in an enhanced level of mineral dissolution, where the highest concentrations of Mg and Ca ions were 88.1 and 63 ppm, respectively. The metal ion concentrations decreased with time likely because of the formation of passivating layers. SEM analysis of the rock samples did not indicate in-situ CO_2 mineralization in Case #1.

The other dynamic experiment with CO_2 nanobubble dispersion in 30.2 wt% sodium formate solution (Case #2) confirmed an even greater level of mineral dissolution than Case #1. The highest concentrations

were 407 and 504 ppm for Mg and Ca ions, respectively. Unlike Case #1, the mineral dissolution did not diminish with increasing throughput of the injection fluid in Case #2, although the CO_2 concentration in the fluid in Case #2 (1.09 mol/L) was smaller than that in Case #1 (1.75 mol/L). SEM analysis of the basaltic rock samples after the experiment in Case #2 identified carbonate minerals, such as vaterite and hydromagnesite, which were not present before the experiment.

Mineral dissolution is a necessary step for the subsequent CO_2 mineralization and the results showed that the enhanced mineral dissolution in Case #2 enabled the direct observation of in-situ CO_2 mineralization in this research. The enhanced mineral dissolution by sodium formate solutions was validated separately by static mineral dissolution experiments.

Introduction

The global CO_2 concentration in the atmosphere has increased to 421 ppm in 2022, which is an increase of 50% since the Industrial Revolution (NOAA, 2022). Among various techniques to reduce carbon emissions, carbon capture, utilization, and storage (CCUS) is considered crucial toward carbon neutrality and addressing the long-term climate challenge (Zhao et al. 2023; Zhang and DePaolo, 2017).

Ultramafic and mafic rocks hold great potential for ex-situ and in-situ CO_2 mineralization (Luhmann et al., 2017). In particular, basaltic rocks are widely distributed: most of the ocean floor, about 70% of the Earth's surface, and more than 5% of the continents are basaltic (Snæbjörnsdóttir et al., 2020). They are abundant in reactive Ca- and Mg-rich minerals, such as pyroxene and olivine (Raza et al., 2022), which can react rapidly with CO_2 for CO_2 mineralization.

Geological CO_2 sequestration in (ultra)mafic rock formations can expect the mineralization trapping mechanism, which is one of the four major CO_2 trapping mechanisms: the structural, capillary, solubility, and mineralization trapping mechanisms. The solubility and mineralization trapping mechanisms are considered more secure than the first two, which rely largely on the petrophysical properties of the formation (De Silva et al., 2015). There have been two carbon sequestration projects in basaltic rock formations: CarbFix (Gislason et al., 2010) and Wallula (B.P. McGrail et al. 2011; McGrail et al., 2017). The CarbFix project injected CO_2-saturated water (carbonated water) into basaltic rocks. Approximately 25 tonnes of water was needed to dissolve 1 tonne of CO_2 based on the CO_2 solubility (Snæbjörnsdóttir et al., 2020). Tracer and isotope analysis showed that more than 95% of the injected CO_2 was mineralized within 2 years of the injection. To date, no injectivity issue has been observed. The Wallula project started injecting liquid CO_2 into the basaltic rocks in 2013. The bulk CO_2 phase was trapped by the cap rock, but a portion of the injected CO_2 was mineralized after two years according to core analysis. No quantitative results were reported. These two projects demonstrate the potential that basaltic formations are suitable for secure geological CO_2 sequestration.

Geochemical reactions between CO_2 and basaltic rocks have been studied by many researchers. The studies can be divided into two types of experiments: batch and flow-through experiments. In batch experiments, CO_2 and basaltic rocks are vigorously mixed in a closed system. For example, Schaef et al. (2011) performed batch experiments with different types of basaltic rocks. Their results indicated that basaltic rocks with similar compositions can result in significantly different levels of reactivity and mineralization. Voigt et al. (2021) found that approximately 20% of the injected CO_2 was mineralized after 5 months under an enhanced CO_2 partial pressure and 130°C. Xiong et al. (2017) conducted batch experiments with fractured and unfractured basaltic cores. They observed mineral carbonation as early as six weeks after the commencement of the experiment, where the main secondary minerals were Ca-Mg-Fe carbonate at 150°C. Contrary to batch experiments, flow-through experiments result in dynamic reaction processes between CO_2 and basaltic rocks when CO_2 flows through basaltic rocks. For injectivity and reaction kinetics, such experiments can use crushed rock samples. Marieni et al. (2020) continuously injected CO_2 into crushed basaltic rocks while collecting the excess CO_2 from the outlet. The basaltic rock dissolution rate was determined by measuring the Ca and Si concentrations. One of the most important

conclusions from Marieni et al. (2020) is that the formation of passivation layers likely resulted in incongruent dissolution, in which the Ca concentration reached a steady state, but the Si concentration continued to increase. Menefee et al. (2018) demonstrated that mineral carbonation typically occurred where divalent ions were abundant. Also, increasing bicarbonate ions contributed to the CO_2 mineralization. Most of the previous experiments required weeks or even months to observe CO_2 mineralization. Studies have shown that the rate-limiting step is the dissolution of silicate minerals induced by a reduced pH upon CO_2 dissolution in water (Marini, 2007; Abdolhosseini Qomi et al., 2022). The formation of passivation layers also limited the reactions between rock surfaces and CO_2 (Marieni et al., 2020; Daval et al., 2013; Béarat et al., 2006).

CO_2 mineralization in (ultra)mafic rocks is considered to occur in two steps: dissolution of silicate minerals and CO_2 mineralization. The mineral dissolution step is promoted by proton or ligands (Abdolhosseini Qomi et al., 2022). Proton-promoted dissolution occurs when protons attack the metal-oxygen-silicate bridging bonds and can be enhanced by increasing the level of CO_2 saturation. Wang et al. (2023a) presented that aqueous nanobubble dispersion of CO_2 can increase the level of supersaturation of the water phase by CO_2, in which nanoscale bubbles of CO_2 are dispersed in the external water phase that is molecularly supersaturated by CO_2 (Thi Phan et al., 2020; Zhou et al., 2021; Achour et al. 2023). Wang et al. (2023a) showed that the level of supersaturation by aqueous nanobubble dispersion increased with increasing the system pressure up to 208 bara. Ligand-promoted dissolution involves ligating metal cations (Abdolhosseini Qomi et al., 2022); for example, sodium formate solutions enhanced the kinetics and level of calcite dissolution in Wang et al. (2023b) and Oyenowo et al. (2023). As shown in Wang et al. (2023a), it is possible to generate CO_2 nanobubble dispersion in sodium formate solution; therefore, this paper presents an experimental study of potential synergy using the two mineral-dissolution mechanisms.

One method to promote the CO_2 mineralization step is pH swing (Azdarpour et al., 2015; Stokreef et al., 2022), in which the solution pH is increased after the mineral dissolution stage to promote the generation of carbonate minerals. Many studies were performed using such a pH swing (Sanna et al., 2013; Hemmati et al., 2014; Teir et al., 2007). In this research, a NaOH solution was used to swing the solution pH. Note that engineered methods for the CO_2 mineralization step are important only when the mineral dissolution step is properly designed as the necessary first step.

The main objectives of this research were to study aqueous nanobubble dispersion of CO_2 in sodium formate solution for enhanced CO_2 mineralization using basaltic rocks. The CO_2 concentrations of aqueous nanobubble dispersions were measured in deionized (DI) water at pressures up to 208 bara and in aqueous solution of 30.2 wt% sodium formate (20.0 wt% formate) at 139 bara at 75°C. High-temperature batch experiments were performed to study the enhancement of mineral dissolution by formate ion as a ligand. Finally, dynamic CO_2 mineralization experiments were conducted by CO_2 nanobubble dispersion in DI water and sodium formate solution. This is the first time aqueous nanobubble dispersion of CO_2 and sodium formate solution were studied for CO_2 mineralization.

Methods

This section presents the materials and experimental procedures for investigating the enhanced CO_2 mineralization by CO_2 nanobubble dispersion and sodium formate solution. It consists of characterization of basaltic rock samples, generation and CO_2 content measurements of aqueous nanobubble dispersions, static mineral dissolution experiments, and dynamic CO_2 mineralization experiments.

Materials

Basaltic rock samples (Kocurek Industries Inc.) were crushed into fine particles, the size of which varied for different experiments in this research. The crushed samples were ultrasonically cleaned for 10 minutes to remove finer particles. Then, the wet samples were dried overnight in an oven at 75°C before they were ready for dissolution or mineralization experiments. The dried samples were characterized by scanning electron microscopy (SEM) and X-ray diffraction analysis (XRD). Figure 1 shows the XRD spectrum of the rock samples used in this research. Table 1 shows the initial composition of the rock samples.

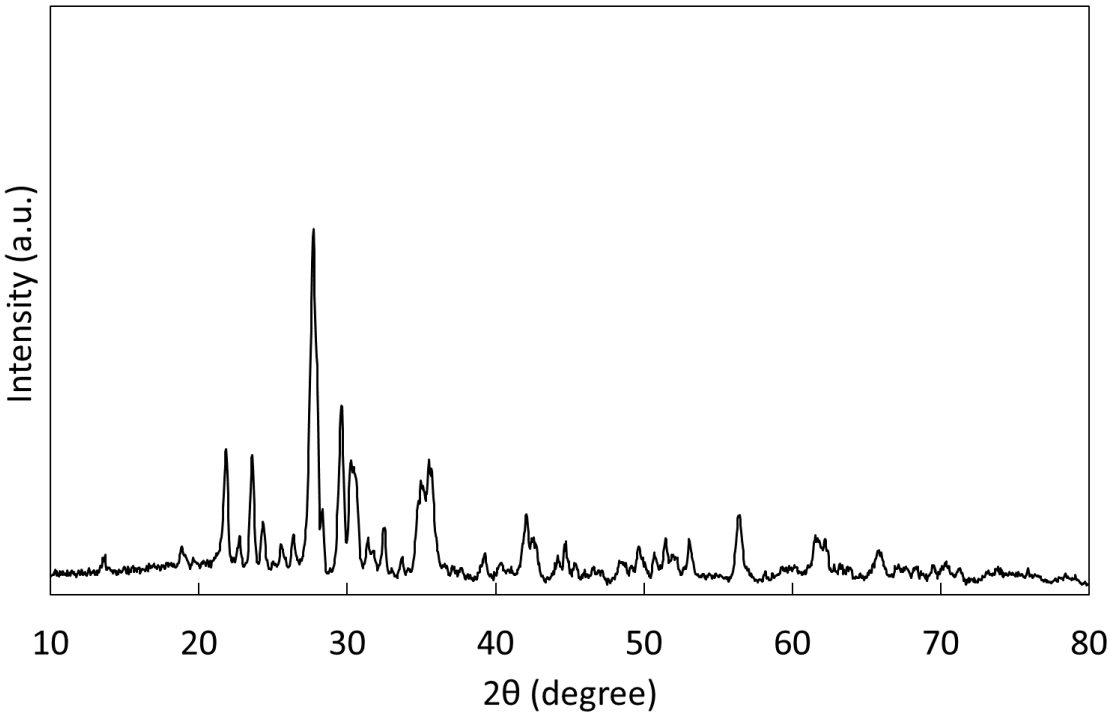

Figure 1 XRD patterns of the original basaltic rock sample. Table 1 gives the composition.

Table 1 Initial composition of the basaltic rock sample used in this research.

Mineral	Formula	Weight percent, %
Anorthite	$CaAl_2Si_2O_8$	38
Albite	$Na_{0.998}K_{0.002}AlSi_3O_8$	23
Enstatite	$Fe_{0.249}Mg_{0.751}SiO_3$	27.8
Diopside	$CaMgSi_2O_6$	11.1

The DI water used to prepare solutions in this research had a resistivity of 18.2 MΩ·cm. The CO_2 used in this research had a purity greater than 99%. Stainless-steel porous membranes with an average pore size of 5 μm were used for the generation of CO_2 nanobubble dispersions. The sapphire cell with a total volume of 15.37 mL was used to measure the CO_2 content of aqueous nanobubble dispersions. Sodium formate (Thermo Fisher Scientific, purity: 99%) provided the ligand (i.e., formate) in mineral dissolution and CO_2 mineralization experiments. The experiments in this research were conducted at 75°C to enhance the kinetics of mineral dissolution.

CO_2 content measurement of CO_2 nanobubble dispersion

Figure 2 shows the experimental setup for measuring the CO_2 content of aqueous nanobubble dispersions in this research. The detailed experimental procedure can be found in Wang et al (2023a). Since the measurement was performed at 75°C in this research, the collected water from the accumulator 2f could lose part of the mass, resulting in an underestimated CO_2 content. To avoid this experimental uncertainty, the volume of CO_2 in the accumulator 2f was directly measured. To this end, the piston was pushed back to the top after each experiment and the injection volume was obtained by recording the change in pump volume.

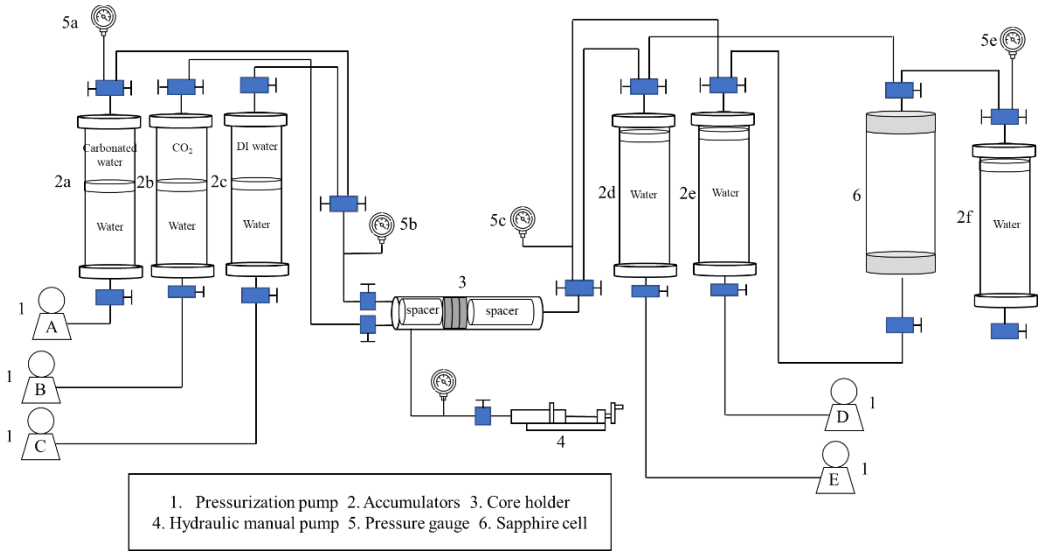

Figure 2 Experimental setup for measuring the gas content of aqueous CO_2 nanobubble dispersion. The experimental procedure was described by Wang et al. (2023a).

Two liquids were used for CO_2 content measurements: DI water and 20.0 wt% formate solution (i.e., 30.2 wt% sodium formate solution). The composition of the latter was 102110 ppm Na^+ and 200000 ppm $HCOO^-$. The injection pressure of both cases was 138.9 bara (2000 psig). The total flow rate for the CO_2 and aqueous fluid was 100 mL/hr with the equal-volume mixing ratio.

Static mineral dissolution experiments

Static mineral dissolution experiments were conducted at 75°C and atmospheric pressure to investigate the effect of formate as a ligand on mineral dissolution. The basaltic rocks were crushed and sieved to obtain the 106-150 μm fraction. The crushed sample was rinsed with DI water at least three times and then ultrasonically cleaned for ten minutes to remove fine particles. After that, 2.0 g of the sample was added to a high-temperature vial. The vials were subjected to a rigorous leakage test prior to the experiments to avoid any water evaporation. Figure 3 shows the five fluids used: DI water, 5.0 wt%, 10.0 wt%, 20.0 wt% and 30.0 wt% formate solutions (i.e., 7.55 wt%, 15.1 wt%, 30.2 wt%, and 45.3 wt% sodium formate solutions). For each, 30 mL was added to the vial. Therefore, the fluid-solid ratio (15 mL/gram) was consistent for all the cases.

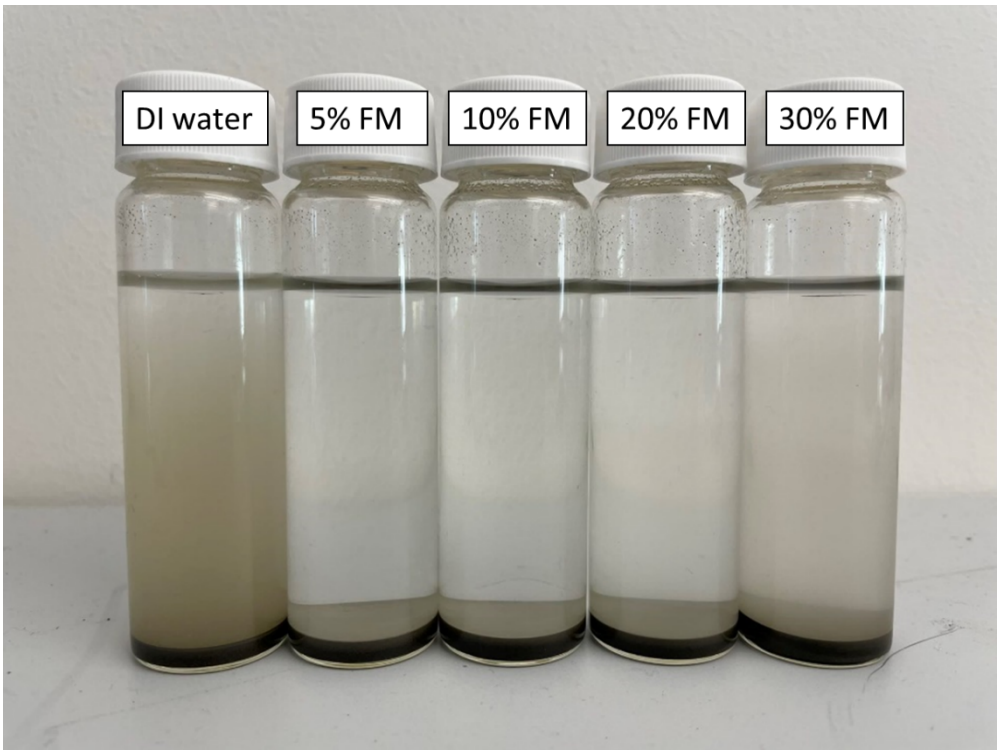

Figure 3 Mineral dissolution with DI water and formate solutions. A constant fluid-solid ratio of 15 mL/g was used throughout the experiments.

The pH and ion (Mg, Al, Si, K, Ca, and Fe) concentrations were monitored by sampling at different times. Each sampling extracted only 0.3 mL of the solution from the vial so that the fluid-solid ratio did not substantially change. The solution was filtered by a 0.22-μm syringe filter and 0.1 mL of the filtered solution was immediately diluted by 2% nitric acid for ion concentration measurement. The rest of the samples were subjected to pH measurement by a pH meter. The experiments were repeated until the solution pH was stable.

Dynamic mineral dissolution and CO_2 mineralization experiments

Figure 4 shows the experimental setup used for dynamic mineral dissolution and CO_2 mineralization experiments. The two parts correspond to the nanobubble-generation and carbon-mineralization systems. The nanobubble generation system was similar to that in section 2.2, but the sapphire cell was not needed for gas content measurement. The generated nanobubble sample was stored in the accumulator 2f. Note that the accumulator 2f was rotated 180° in comparison to the previous experiments in order to avoid injecting the CO_2 gas that may be produced from the CO_2 nanobubble dispersion. The CO_2 mineralization system consisted of a stainless-steel sandpack, which was one inch in inner diameter and six inches in length, a back pressure regulator (BPR), and an accumulator filled with N_2 to provide back pressure. Two pressure gauges were used to measure the upstream and downstream pressures of the sandpack.

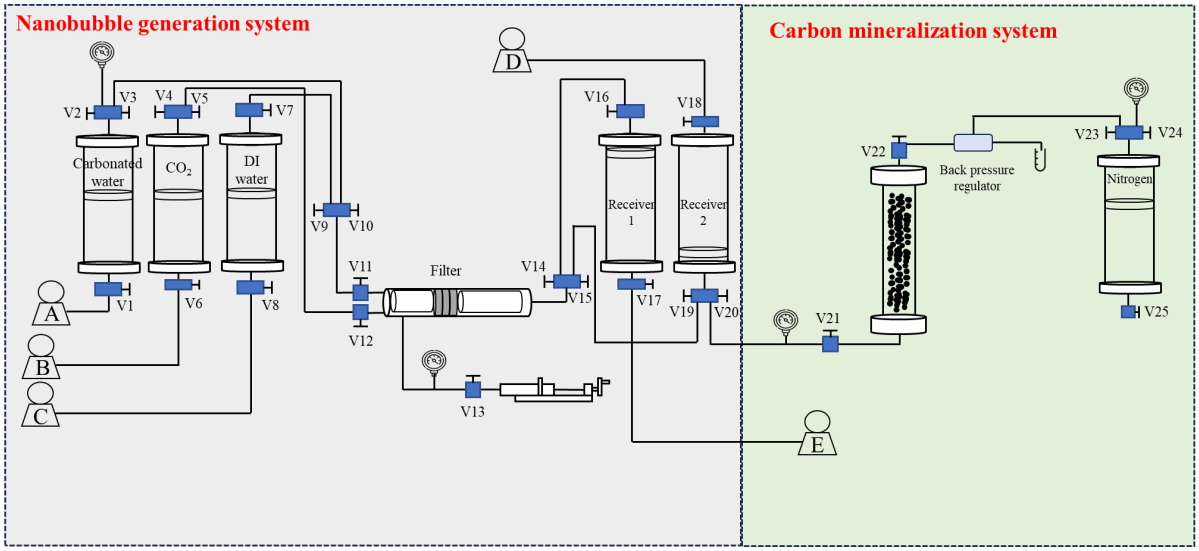

Figure 4 Experimental setup for dynamic mineral dissolution and CO_2 mineralization experiments. The experimental procedure was described in the section on "dynamic mineral dissolution and CO_2 mineralization experiments."

The crushed rock samples were sieved to obtain the 1-2 mm size fraction. Finer rock samples were preferred for the chemical reaction kinetics, but they were not used to avoid any potential clogging issues with the tubing. Each sandpack used 18.0 g of the crushed rock sample and was tested for leakage. Then, the system was filled with DI water and pressurized to the pressure of the CO_2 nanobubble sample. The back pressure was set to be 3.4 bar (50 psi) greater than the injection pressure. This small pressure difference was chosen to control the properties of the CO_2 nanobubble dispersion during the experiment. The effluents were collected by the graduated vials, and the pH was measured immediately after changing the vials. The solution was filtered by a 0.22-μm syringe filter and 0.1 mL of the collected solution was immediately diluted by 2% nitric acid for ion concentration measurement. Note that the Fe concentration was not considered in this research because it also could come from the stainless-steel container and tubing. After the above analysis, 0.5 mL of 1 mol/L NaOH solution was added to the rest of the samples for a pH swing. The samples were completely dried, and the precipitates were further analyzed.

Table 2 summarizes the experimental conditions. The experiments were divided into two stages: mineral dissolution and CO_2 mineralization. For the mineral dissolution stage, nanobubbles in DI water or 20 wt% formate solution reacted with rock samples. The 30 wt% formate solution was not used because the CO_2 might cause salt precipitation (drying out) near the solubility limit. Sodium formate solutions tend to suppress the reduction in solution pH owing to CO_2 dissolution as buffer solutions. That is, during the mineral dissolution stage, the solution pH in Case #2 was expected to be greater than that in Case #1. The residence time (the duration allowed for chemical reactions during the experiment) was estimated to be three hours based on the injection flow rate, sandpack volume, and rock mass. For the CO_2 mineralization stage, 1.0 mol/L NaOH solution was injected to adjust the in-situ solution pH. After the experiment, the system was depressurized, and the rock sample was completely dried for SEM analysis.

Table 2 Experimental conditions for dynamic mineral dissolution and CO_2 mineralization experiments. The experiments were divided into two stages: the dissolution and mineralization stages. The experimental temperature was 75°C.

	Case #1	Case #2
Dissolution stage	CO_2 nanobubble in DI water was injected at 5 mL/hr for 100 mL at 138.9 bara (2000 psig)	CO_2 nanobubble in 20 wt% formate solution was injected at 5 mL/hr for 100 mL at 138.9 bara (2000 psig)
Mineralization stage	1.0 mol/L NaOH solution was injected at 5 mL/hr for 20 mL at 144.1 bara (2075 psig)	1.0 mol/L NaOH solution was injected at 5 mL/hr for 20 mL at 144.1 bara (2075 psig)

Results and discussion

CO_2 content measurement of CO_2 nanobubble dispersion

Figure 5 shows the CO_2 content in CO_2 nanobubble dispersions with DI water and 20 wt% formate solution at 75°C. As a reference, the red line represents the inherent solubilities of CO_2 in DI water (with no nanobubbles) at 75°C calculated using Phreeqc (Parkhurst et al., 2013). The CO_2 concentration in the nanobubble dispersion with DI water was measured to be 1.75 mol/L at 138.9 bara, which was 65% greater than the inherent solubility of CO_2 at the same pressure. This solubility enhancement was close to, but slightly greater than that at room temperature reported by Wang et al (2023a).

The CO_2 concentration in CO_2 nanobubble dispersion with 20 wt% formate solution was smaller than that with DI water because of the higher salinity. The CO_2 concentration was measured to be 1.09 mol/L, which was close to the CO_2 solubility in DI water under the same conditions. Note however that formate species generated by captured CO_2 is viewed as a carbon carrier that is highly soluble in brine (Oyenowo et al., 2021; Baghishov et al., 2022; Breunig et al., 2023; Wang et al., 2023b; Oyenowo et al., 2023; Oyenowo et al., 2023). If we considered the contribution from formate ions, 5.25 mol/L, the CO_2 nanobubble dispersion with 20 wt% formate solution had a carbon concentration of 6.34 mol/L [i.e., (1.09 + 5.25) mol/L]. Also, the CO_2 nanobubble dispersion in 20 wt% formate solution should have a higher pH than that in DI water, favorably affecting the stability of CO_2 nanobubbles because the adsorption of OH^- on the nanobubble surfaces is expected to increase the electrostatic repulsion between nanobubbles (Nirmalkar et al., 2018; Alam et al., 2021; Antonio Cerrón-Calle et al., 2022; Prakash et al., 2023).

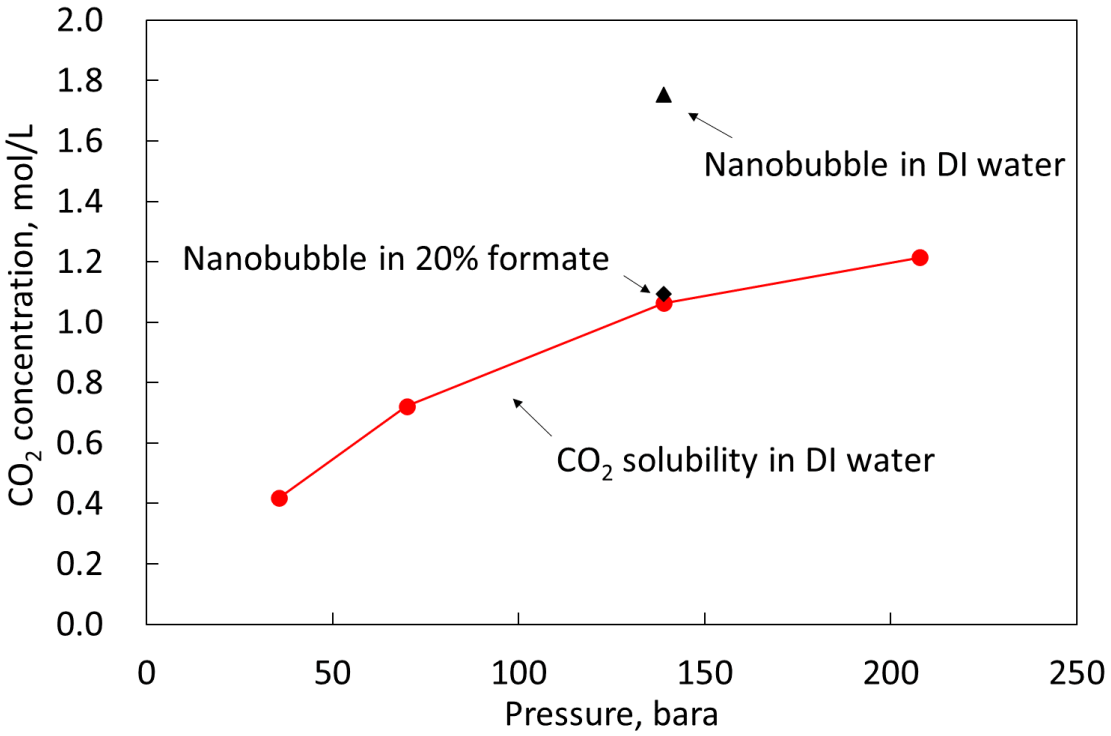

Figure 5 Gas content in CO_2 nanobubble dispersions at 75°C. The red line is the CO_2 solubility in DI water based on Phreeqc. The triangle is the gas content of CO_2 nanobubbles in DI water. The square is the gas content of CO_2 nanobubbles in 20 wt% formate solution.

Static mineral dissolution experiments

Figure 6 presents the pH histories from the static mineral dissolution experiments. The duration of the experiments was 291 hours. The DI-water case showed an increase in solution pH, resulting from the dissolution of silicate minerals because of silicate anion (SiO_4^{4-}) in the water phase. Formate solutions resulted in a reduction in solution pH because formate ions made complexes with metal ions upon the dissolution of silicate minerals. The dissolution rate was reduced over time, resulting in a stable pH value as shown in Figure 6.

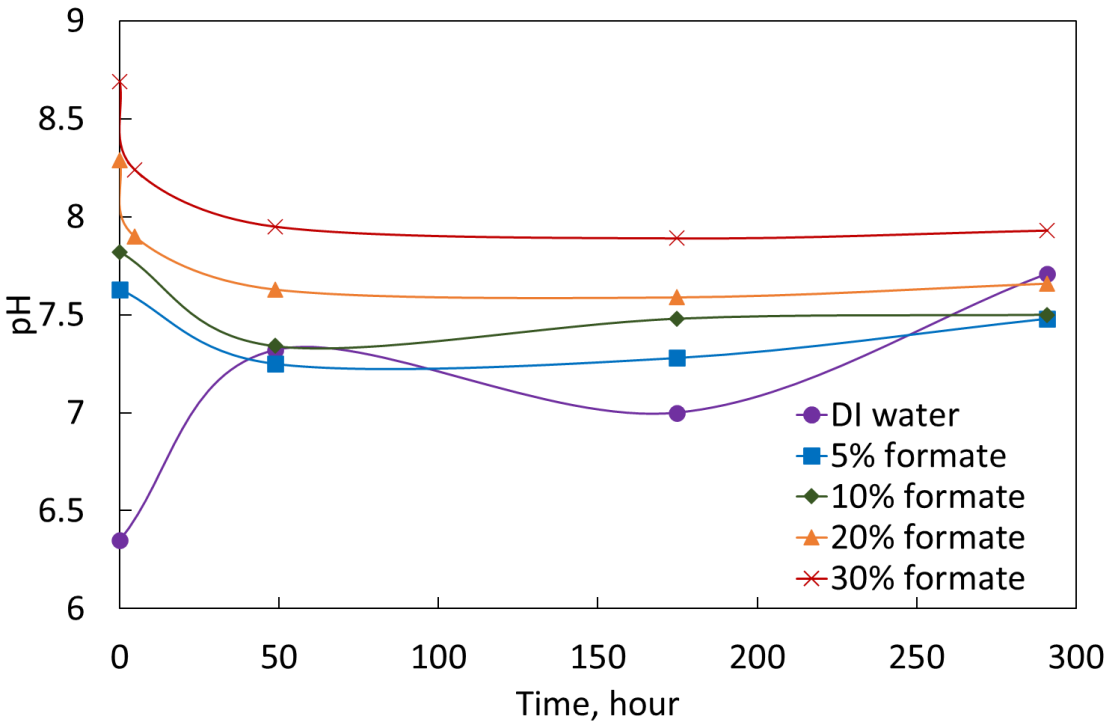

Figure 6 pH history of static mineral dissolution experiments. DI water, 5%, 10%, 20% and 30% formate cases were reported.

Figure 7 represents the concentrations of metal ions in the five cases. DI water dissolved a small amount of silicate minerals, and the concentrations of metal ions were mostly less than 10 ppm. The dissolution was controlled by the solubility product constants of silicate minerals at 75°C. In formate solutions, however, the concentrations of metal ions increased significantly, which indicated that formate could enhance the ligand-promoted dissolution of silicate minerals. The concentrations of Mg, Si, K, and Ca ions were particularly high, demonstrating the selective dissolution of the basalt sample used. Ca and Mg ions were important because they were essential for the formation of insoluble carbonate minerals for CO_2 mineralization. Overall, the ion concentrations increased with formate concentration, but some points deviated from this trend; for example, 5% formate solution led to the highest Ca concentration at 48.7 hours. The reason for this outlier is unclear upon the preparation of this manuscript.

The mechanism of enhanced mineral dissolution by formate was discussed by Oyenowo et al. (2023). Metal ions can form both unidentate and bidentate complexes with formate, to which the enhanced level of silicate mineral dissolution observed in this research can be attributed. Then, these dissolved metal ions become available for carbonation reactions with carbonate ions from dissolved CO_2. Controlling geochemical conditions for such mineralization reactions is the next step after the enhanced dissolution of silicate minerals increases the concentrations of multivalent cations, such as Ca and Mg ions.

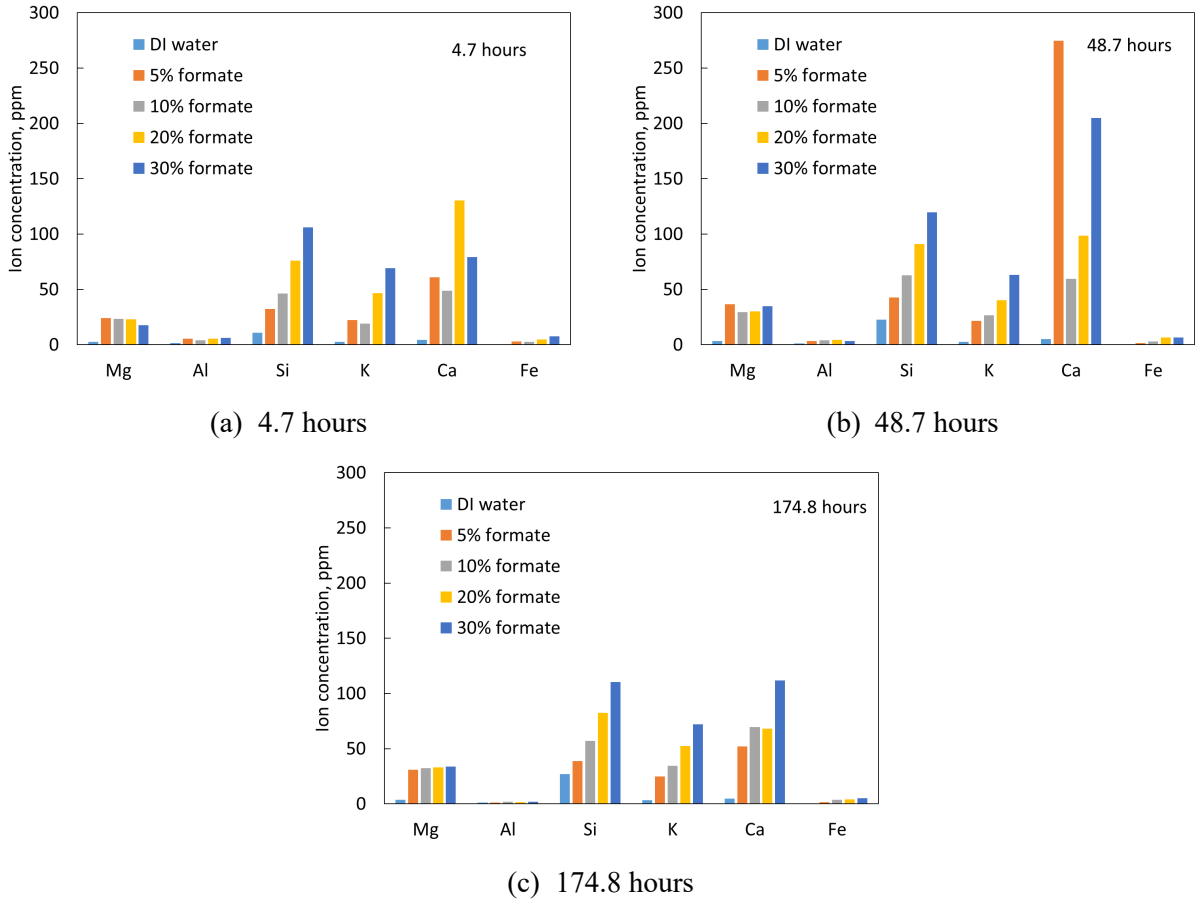

(a) 4.7 hours

(b) 48.7 hours

(c) 174.8 hours

Figure 7 Ion concentration of static mineral dissolution experiments at (a) 4.7 hours, (b) 48.7 hours, and (c) 174.8 hours.

Dynamic mineral dissolution and CO_2 mineralization experiments

Figure 8 shows the pH and ion concentrations of the effluent samples in Case #1 (Table 2). The first two effluent samples represented reactions between DI water and rock samples because the system was initially saturated with DI water. Therefore, the solution pH increased to 7.36 and the Mg and Ca concentrations were below 5 ppm. The Si concentration reflected the total dissolution of silicates, and it was 37.1 ppm at the cumulative injected volume of 10 mL, which was the beginning of the CO_2 nanobubble stage. Once the CO_2 nanobubble dispersion was injected, the pH of the effluent solutions gradually decreased to 6.35; therefore, the concentration of bicarbonate ion (HCO_3^-) was much greater than those of H_2CO_3 and CO_3^{2-}. The Mg and Ca concentrations significantly increased to their peak values: 88.1 ppm for Mg and 63 ppm for Ca. The Si concentration, however, gradually increased to approximately 53 ppm and stabilized. The stable Si concentration indicated a steady state of interactions between the CO_2 nanobubble dispersion and the rock samples. Then, the Ca and Mg concentrations gradually decreased until the end of the CO_2 nanobubble stage. This decreasing trend may be because the formation of passivation layers suppressed further dissolution reactions, but more analysis is needed to confirm that possibility. As the NaOH stage started, the solution pH rapidly increased. The Mg and Ca concentrations increased because the system had been shut in for 12 hours before the CO_2 mineralization stage (i.e., a longer residence time). Then, the ion concentrations decreased to a low level of less than 5 ppm, while the Si concentration rapidly increased as shown in Figure 8d. This indicated that high-pH

alkaline solutions did not effectively dissolve Ca- and Mg-containing silicate minerals under the experimental conditions in this research.

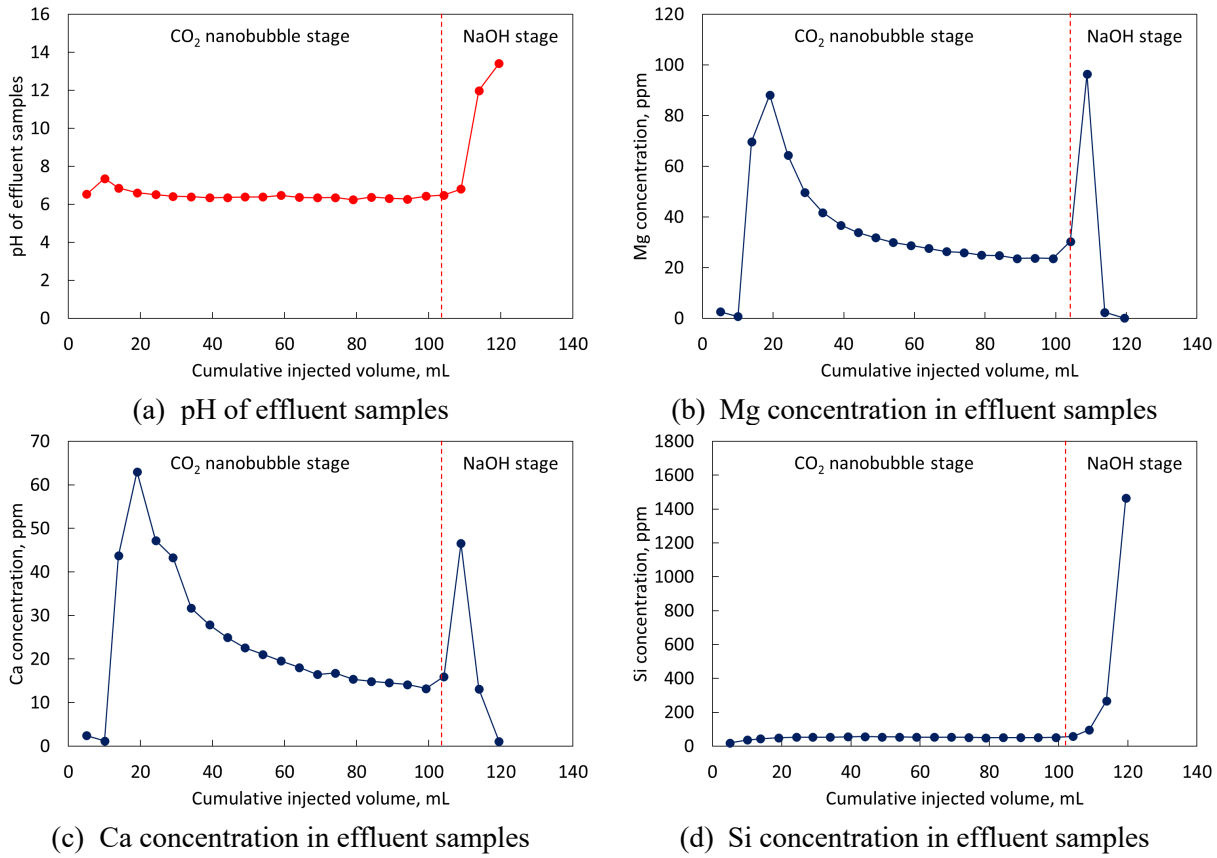

(a) pH of effluent samples

(b) Mg concentration in effluent samples

(c) Ca concentration in effluent samples

(d) Si concentration in effluent samples

Figure 8 pH and ion concentrations of effluent samples in Case #1. The pH was measured by a pH meter. The ion concentrations were measured by ICP-MS.

The dried effluent samples were subjected to XRD to analyze their compositions. The results in Figure 9 showed that the dominant compound was Na_2CO_3. The Ca and Mg concentrations were so small that their carbonate minerals were not detected by XRD.

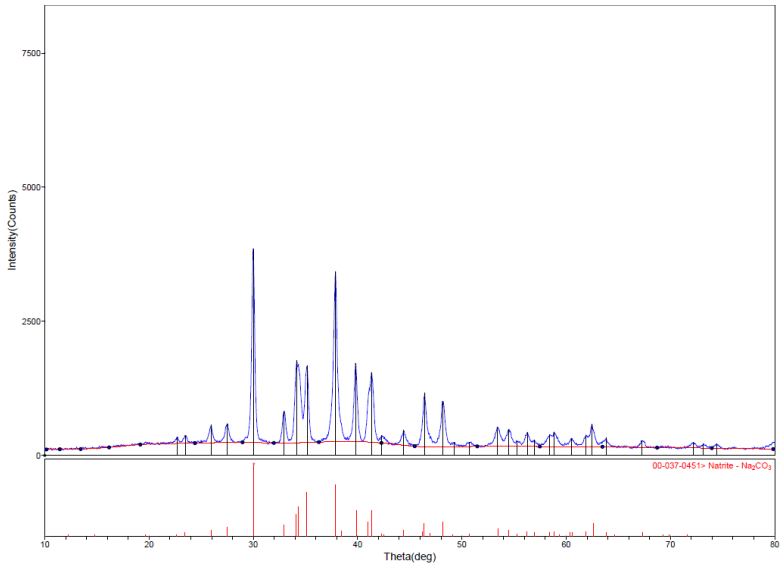

Figure 9 XRD results for the effluent samples in Case #1. The main composition of the effluent sample was sodium carbonate.

Figure 10 shows the SEM images of the crushed rock samples before and after the experiment in Case #1. Initially, small pieces of silicate minerals covered the rock surface (Figure 10a); however, the CO_2 nanobubble injection made the rock surfaces smoother (Figure 10b). No secondary minerals (carbonate minerals) were observed on the rock surface after the experiment. In Case #1 the mineral dissolution was confirmed, but no apparent CO_2 mineralization was observed likely because the Ca and Mg concentrations were small in the experiment as reported in Figure 8. A greater level of mineral dissolution would be necessary to observe the carbon mineralization under the experimental conditions in this research. Increasing the residence time (three hours in this research) is a possible way to increase the level of mineral dissolution and the subsequent CO_2 mineralization as can be seen in the increased concentrations of Mg and Ca ions right after switching to the NaOH injection in Figure 8.

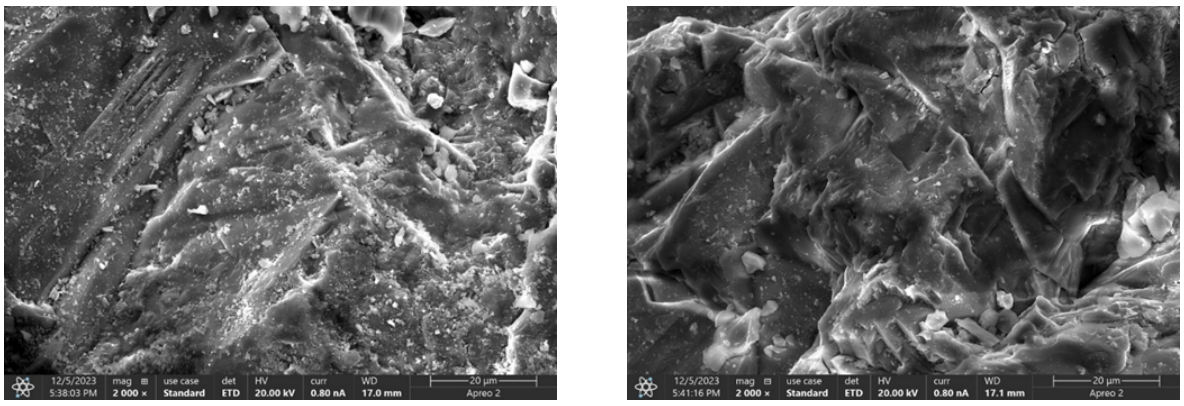

(a) Before the experiment (b) After the experiment

Figure 10 SEM images of the crushed rock sample in Case #1 before (a) and after (b) the experiment. Initially, small pieces of silicate minerals covered the rock surface (Figure 10a). The CO_2 nanobubble injection made the rock surfaces smoother (Figure 10b). No secondary minerals (carbonate minerals) were observed on the rock surface after the experiment.

Figure 11 shows the pH and ion concentrations of the effluent samples in Case #2. The solution pH of the effluents behaved in a similar way to Case #1. However, the ion concentrations were much greater than those in Case #1. The highest concentrations were 407 and 504 ppm for the Mg and Ca ions, respectively.

Interestingly, the Mg and Ca concentrations did not decrease with time (unlike Case #1), but stabilized at approximately 115 and 140 ppm, respectively. This indicated a greater level of the dissolution of silicate minerals with the CO_2 nanobubble dispersion in sodium formate solution even though its CO_2 content was smaller than that that in the nanobubble dispersion with DI water (Figure 5). There are at least three possible reasons for the enhanced mineral dissolution observed in Case #2 in comparison to Case #1. First, the ligand-promoted mechanism of mineral dissolution occurred with a high concentration of formate as a ligand. Second, a greater pH in Case #2 enhanced the stability of CO_2 nanobubbles in the in-situ solution so that the supersaturation of the aqueous phase by CO_2 could enhance the proton-promoted mechanism. Third, the supersaturation by CO_2 reduced the solution pH such that formic acid contributed to an additional mechanism of silicate mineral dissolution.

The dried effluent samples were analyzed by XRD, but the high concentration of sodium formate made it difficult to detect carbonate minerals. Figure 12 shows the SEM images of the crushed rock samples after the experiment in Case #2. Carbonate minerals, such as vaterite and hydromagnesite, were observed on the rock surfaces, which validated the in-situ CO_2 mineralization in Case #2 using the CO_2 nanobubble dispersion in sodium formate solution.

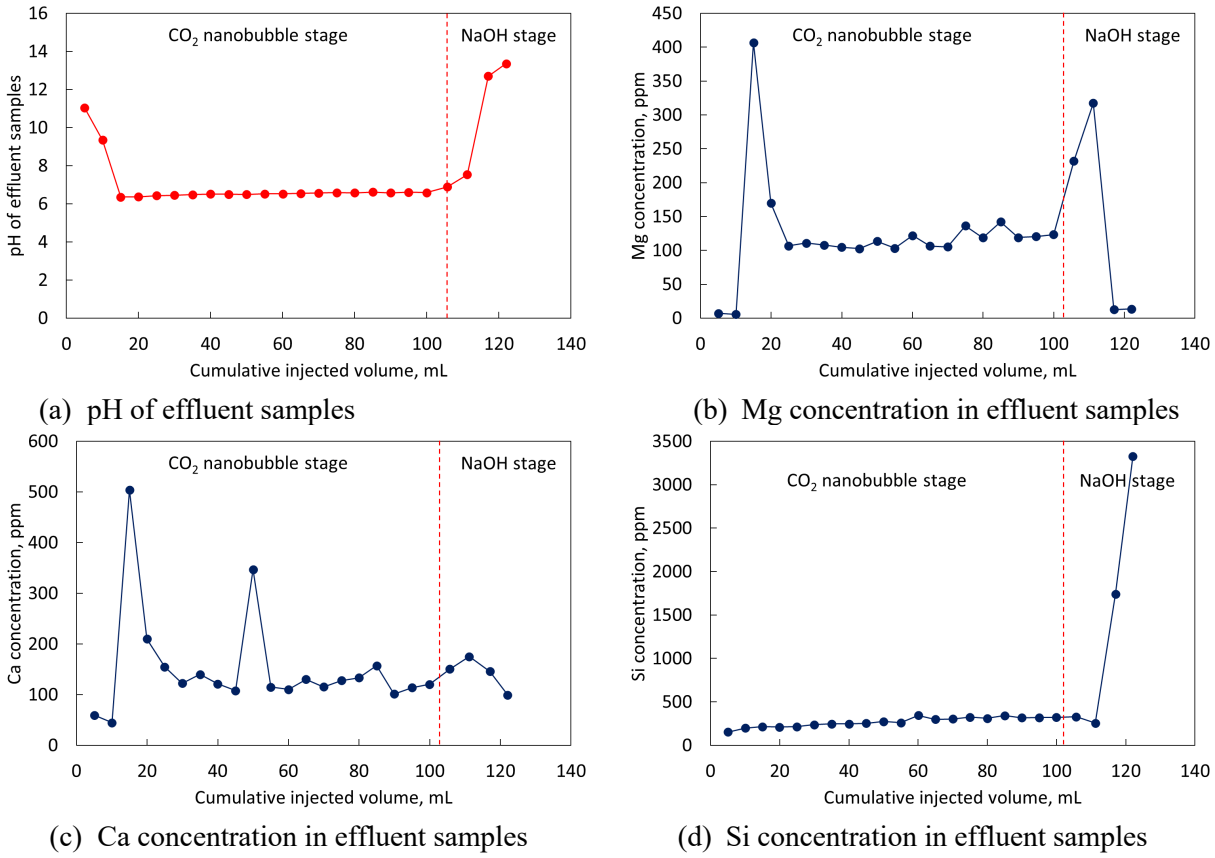

(a) pH of effluent samples

(b) Mg concentration in effluent samples

(c) Ca concentration in effluent samples

(d) Si concentration in effluent samples

Figure 11 pH and ion concentrations of the effluent samples in Case #2. The pH was measured by a pH meter. The ion concentrations were measured by ICP-MS.

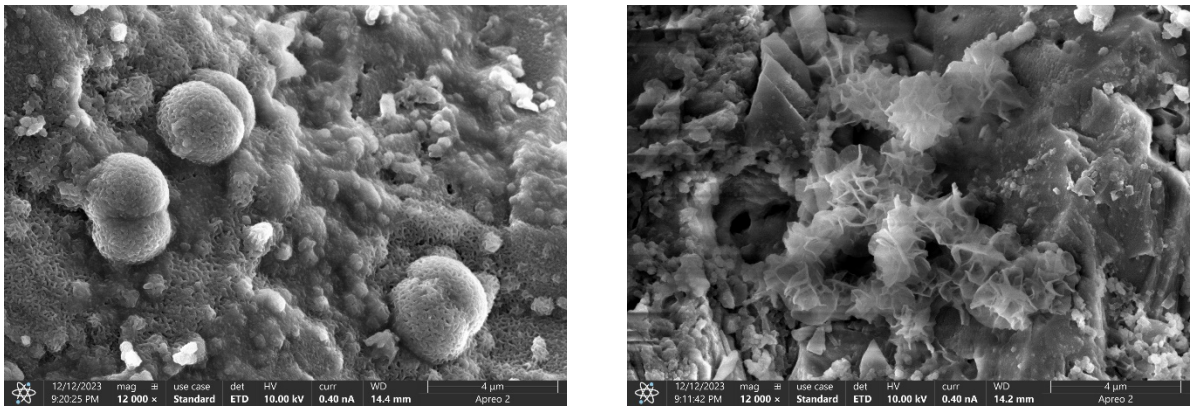

(a) Vaterite (b) Hydromagnesite

Figure 12 SEM images of the crushed rock samples in Case #2 after the experiment. Secondary minerals were observed: (a) vaterite and (b) Hydromagnesite.

Conclusions

This paper presented an application of CO_2 nanobubble dispersion in 30.2 wt% sodium formate solution (20.0 wt % formate) to enhance CO_2 mineralization with basaltic rock samples. The main conclusions are as follows:

1. The aqueous nanobubble dispersion of CO_2 in DI water at 75°C had a CO_2 concentration of 1.75 mol/L at 138.9 bara. This is approximately 65% greater than the inherent solubility of CO_2 at the sample pressure and temperature. The CO_2 concentration decreased to 1.09 mol/L for the CO_2 nanobubble dispersion in 30.2 wt% sodium formate solution at 75°C and 138.9 bara because of the adverse effect of salinity on CO_2 solubility.
2. The static mineral dissolution experiments validated enhanced levels of mineral dissolution for sodium formate solutions by the ligand-promoted mechanism. Such enhancement was observed for Mg, Si, K and Ca ions. Ca and Mg ions are particularly important for the formation of insoluble carbonate minerals in the subsequent CO_2 mineralization step.
3. The dynamic flow-through experiments with CO_2 nanobubble dispersion in DI water (Case #1) resulted in an enhanced level of mineral dissolution, where the highest concentrations for Mg and Ca ions were 88.1 and 63 ppm, respectively. The metal ion concentrations decreased with time likely because of the formation of passivating layers. SEM analysis of the rock samples did not indicate in-situ CO_2 mineralization in Case #1.
4. The other dynamic experiment with CO_2 nanobubble dispersion in 30.2 wt% sodium formate solution (Case #2) confirmed an even greater level of mineral dissolution than Case #1. The highest concentrations were 407 and 504 ppm for Mg and Ca ions, respectively. Unlike Case #1, the mineral dissolution did not diminish with increasing throughput of the injection fluid in Case #2, although the CO_2 concentration in the fluid in Case #2 (1.09 mol/L) was smaller than that in Case #1 (1.75 mol/L). SEM analysis of the basaltic rock samples after the experiment identified vaterite and hydromagnesite, which were not present initially. This indicates in-situ CO_2 mineralization in Case #2, but further surface analysis is needed to corroborate this observation.
5. Mineral dissolution is a necessary step for the subsequent CO_2 mineralization and the results in this research showed that the enhancement of mineral dissolution in Case #2 enabled the direct observation of in-situ CO_2 mineralization. Mineral dissolution is likely an important factor in

designing of the injection fluid for CO_2 mineralization projects since it affects the amounts of multivalent ions exposed to the injected CO_2.

Acknowledgements

We thank the sponsors of the Energi Simulation Industrial Affiliate Program on Carbon Utilization and Storage (ES Carbon UT) at the Center for Subsurface Energy and the Environment at the University of Texas at Austin. Ryosuke Okuno holds the Pioneer Corporation Faculty Fellowship in the Hildebrand Department of Petroleum and Geosystems Engineering at the University of Texas at Austin.

References

Abdolhosseini Qomi, M.J., Miller, Q.R.S., Zare, S., et al. 2022. Molecular-Scale Mechanisms of CO_2 Mineralization in Nanoscale Interfacial Water Films. *Nature Reviews Chemistry* **6**(9): 598–613. https://doi.org/10.1038/s41570-022-00418-1.

Achour, S.H., Sheng, K., Lawal, T., and Okuno, R. 2023. Thermodynamic Modeling of Aqueous Nanobubble Dispersion. Paper presented at the SPE Annual Technical Conference and Exhibition, October 16 - 18, 2023. https://doi.org/10.2118/215122-MS

Alam, H.S., Sutikno, P., Soelaiman, T.A.F. et al. 2022. Bulk Nanobubbles: Generation Using a Two-Chamber Swirling Flow Nozzle and Long-Term Stability in Water. *Journal of Flow Chemistry* **12:** 161–173. https://doi.org/10.1007/s41981-021-00208-8

Antonio Cerrón-Calle, G., Magdaleno, A.L., Graf, J.C., et al. 2022. Elucidating CO_2 Nanobubble Interfacial Reactivity and Impacts on Water Chemistry. *Journal of Colloid and Interface Science* **607**(1): 720-728. https://doi.org/10.1016/j.jcis.2021.09.033

Azdarpour, A., Asadullah, M., Mohammadian, E., et al. 2015. A Review on Carbon Dioxide Mineral Carbonation through pH-Swing Process. *Chemical Engineering Journal* **279**: 615–630. https://doi.org/10.1016/j.cej.2015.05.064.

Baghishov, I., Abeykoon, G.A., Wang, M., et al. 2022. A Mechanistic Comparison of Formate, Acetate, and Glycine as Wettability Modifiers for Carbonate and Shale Formations. *Colloids and Surfaces A: Physicochemical and Engineering Aspects* **652**: 129849. https://doi.org/10.1016/j.colsurfa.2022.129849.

Béarat, H., McKelvy, M.J., Chizmeshya, A.V.G., et al. 2006. Carbon Sequestration via Aqueous Olivine Mineral Carbonation: Role of Passivating Layer Formation. *Environmental Science & Technology* **40**(15): 4802–4808. https://doi.org/10.1021/es0523340.

Breunig, H. M., Rosner, F., Lim, T.-H., and Peng, P. 2023. Emerging Concepts in Intermediate Carbon Dioxide Emplacement to Support Carbon Dioxide Removal. *Energy & Environmental Science* **16**(5): 1821–1837. https://doi.org/10.1039/D2EE03623A

Carbon Dioxide Now More than 50% Higher than Pre-Industrial Levels. 2022. National Oceanic and Atmospheric Administration. https://www.noaa.gov/news-release/carbon-dioxide-now-more-than-50-higher-than-pre-industrial-levels.

Daval, D., Hellmann, R., Martinez, I., et al. 2013. Lizardite Serpentine Dissolution Kinetics as a Function of pH and Temperature, Including Effects of Elevated pCO_2. *Chemical Geology* **351**: 245–256. https://doi.org/10.1016/j.chemgeo.2013.05.020.

De Silva, G.P.D., Ranjith, P.G., and Perera, M.S.A. 2015. Geochemical Aspects of CO_2 Sequestration in Deep Saline Aquifers: A Review. *Fuel* **155**: 128–143. https://doi.org/10.1016/j.fuel.2015.03.045.

Gislason, S.R., Wolff-Boenisch, D., Stefansson, A., et al. 2010. Mineral Sequestration of Carbon Dioxide in Basalt: A Pre-Injection Overview of the CarbFix Project. *International Journal of Greenhouse Gas Control* **4**(3): 537–545. https://doi.org/10.1016/j.ijggc.2009.11.013.

Hemmati, A., Shayegan, J., Bu, J., et al. 2014. Process Optimization for Mineral Carbonation in Aqueous Phase. *International Journal of Mineral Processing* **130**: 20–27. https://doi.org/10.1016/j.minpro.2014.05.007.

Luhmann, A.J., Tutolo, B.M., Bagley, B.C., et al. 2017. Permeability, Porosity, and Mineral Surface Area Changes in Basalt Cores Induced by Reactive Transport of CO_2-rich Brine. *Water Resources Research* **53**(3): 1908–1927. https://doi.org/10.1002/2016WR019216.

Marieni, C., Matter, J.M., and Teagle, D.A.H. 2020. Experimental Study on Mafic Rock Dissolution Rates within CO_2-Seawater-Rock Systems. *Geochimica et Cosmochimica Acta* **272**: 259–275. https://doi.org/10.1016/j.gca.2020.01.004.

Marini, L. 2007. *Geological Sequestration of Carbon Dioxide - Thermodynamics, Kinetics, and Reaction Path Modeling*. Vol. 11. Developments in Geochemistry. Elsevier. https://doi.org/10.1016/S0921-3198(06)X8011-0.

McGrail, B. Peter, Schaef, H.T., Spane, F.A., et al. 2017. Field Validation of Supercritical CO_2 Reactivity with Basalts. *Environmental Science & Technology Letters* **4**(1): 6–10. https://doi.org/10.1021/acs.estlett.6b00387.

McGrail, B.P., Spane, F.A., Sullivan, E.C., et al. 2011. The Wallula Basalt Sequestration Pilot Project. *Energy Procedia* **4**: 5653–5660. https://doi.org/10.1016/j.egypro.2011.02.557.

Menefee, A.H., Giammar, D.E., and Ellis, B.R. 2018. Permanent CO_2 Trapping through Localized and Chemical Gradient-Driven Basalt Carbonation. *Environmental Science & Technology* **52**(15): 8954–8964. https://doi.org/10.1021/acs.est.8b01814.

Nirmalkar, N., Pacek, A.W., and Barigou, M. 2018. On the Existence and Stability of Bulk Nanobubbles. *Langmuir* **34**(37): 10964–10973. https://doi.org/10.1021/acs.langmuir.8b01163

Oyenowo, O.P., Sheng, K., Abeykoon, G.A., and Okuno, R. 2021. A Case Study of Using Aqueous Formate Solution for Carbon Sequestration and Geological Storage, The GEOGULF 2021 Conference, October 27 – 29, 2021, Austin, Texas. *GCAGS Transactions* **71:** 203 – 215.

Oyenowo, O.P., Sheng, K., and Okuno, R. 2023. Simulation Case Studies of Aqueous Formate Solution for Geological Carbon Storage. *Fuel* **334**: 126643. https://doi.org/10.1016/j.fuel.2022.126643.

Oyenowo, O.P., Wang, H., Okuno, R., et al. 2023. Geochemical Impact on Rock Wettability in Injection of High-Concentration Formate Solution for Enhanced Geologic Carbon Storage and Oil Recovery. In Day 2 Thu, June 29, 2023, D021S010R005. The Woodlands, Texas, USA: SPE. https://doi.org/10.2118/213786-MS.

Parkhurst, D.L., and Appelo, C.A.J., 2013. Description of Input and Examples for PHREEQC version 3—A computer program for speciation, batch-reaction, one-dimensional transport, and inverse geochemical calculations: U.S. Geological Survey Techniques and Methods, Book 6, Chapter A43, 497 p., https://doi.org/10.3133/tm6A43

Prakash, R., Lee, J., Moon, Y., et al. 2023. Experimental Investigation of Cavitation Bulk Nanobubbles Characteristics: Effects of pH and Surface-Active Agents. *Langmuir* **39**(5): 1968–1986. https://doi.org/10.1021/acs.langmuir.2c03027.

Raza, A., Glatz, G., Gholami, R., et al. 2022. Carbon Mineralization and Geological Storage of CO_2 in Basalt: Mechanisms and Technical Challenges. *Earth-Science Reviews* **229**: 104036. https://doi.org/10.1016/j.earscirev.2022.104036.

Sanna, A., Dri, M., and Maroto-Valer, M. 2013. Carbon Dioxide Capture and Storage by pH Swing Aqueous Mineralisation Using a Mixture of Ammonium Salts and Antigorite Source. *Fuel* **114**: 153–161. https://doi.org/10.1016/j.fuel.2012.08.014.

Schaef, H.T., McGrail, B.P., and Owen, A.T. 2011. Basalt Reactivity Variability with Reservoir Depth in Supercritical CO_2 and Aqueous Phases. *Energy Procedia* **4**: 4977–4984. https://doi.org/10.1016/j.egypro.2011.02.468.

Snæbjörnsdóttir, S.Ó., Sigfússon, B., Marieni, C., et al. 2020. Carbon Dioxide Storage through Mineral Carbonation. *Nature Reviews Earth & Environment* **1**(2): 90–102. https://doi.org/10.1038/s43017-019-0011-8.

Stokreef, S., Sadri, F., Stokreef, A., et al. 2022. Mineral Carbonation of Ultramafic Tailings: A Review of Reaction Mechanisms and Kinetics, Industry Case Studies, and Modelling. *Cleaner Engineering and Technology* **8**: 100491. https://doi.org/10.1016/j.clet.2022.100491.

Teir, S., Kuusik, R., Fogelholm, C.-J., et al. 2007. Production of Magnesium Carbonates from Serpentinite for Long-Term Storage of CO_2. *International Journal of Mineral Processing* **85**(1–3): 1–15. https://doi.org/10.1016/j.minpro.2007.08.007.

Thi Phan, K.K., Truong, T., Wang, Y., et al. 2020. Nanobubbles: Fundamental Characteristics and Applications in Food Processing. *Trends in Food Science & Technology* **95**: 118–130. https://doi.org/10.1016/j.tifs.2019.11.019.

Voigt, M., Marieni, C., Baldermann, A., et al. 2021. An Experimental Study of Basalt–Seawater–CO_2 Interaction at 130 °C. *Geochimica et Cosmochimica Acta* **308**: 21–41. https://doi.org/10.1016/j.gca.2021.05.056.

Wang, H., Lawal, T., Achour, S.H., et al. 2023a. Aqueous Nanobubble Dispersion of CO_2 at Pressures Up To 208 Bara. *Energy & Fuels* **37**(24): 19726–19737. https://doi.org/10.1021/acs.energyfuels.3c03660.

Wang, H., Precious Oyenowo, O., and Okuno, R. 2023b. Aqueous Formate Solution for Enhanced Water Imbibition in Oil Recovery and Carbon Storage in Carbonate Reservoirs. *Fuel* **345**: 128198. https://doi.org/10.1016/j.fuel.2023.128198.

Xiong, W., Wells, R.K., Menefee, A.H., et al. 2017. CO_2 Mineral Trapping in Fractured Basalt. *International Journal of Greenhouse Gas Control* **66**: 204–217. https://doi.org/10.1016/j.ijggc.2017.10.003.

Zhang, S., and DePaolo, D.J. 2017. Rates of CO_2 Mineralization in Geological Carbon Storage. *Accounts of Chemical Research* **50**(9): 2075–2084. https://doi.org/10.1021/acs.accounts.7b00334.

Zhao, K., Jia, C., Li, Z., et al. 2023. Recent Advances and Future Perspectives in Carbon Capture, Transportation, Utilization, and Storage (CCTUS) Technologies: A Comprehensive Review. *Fuel* **351**: 128913. https://doi.org/10.1016/j.fuel.2023.128913.

Zhou, L., Wang, S., Zhang, L., et al. 2021. Generation and Stability of Bulk Nanobubbles: A Review and Perspective. *Current Opinion in Colloid & Interface Science* **53**: 101439. https://doi.org/10.1016/j.cocis.2021.101439.